Journal of Solid State Chemistry **156,** 122–134 (2001)
doi:10.1006/jssc.2000.8971, available online at http://www.idealibrary.com on IDEAL®

Cation Ordering Types and Dielectric Properties in the Complex Perovskite $Ca(Ca_{1/3}Nb_{2/3})O_3$

I. Levin,* J. Y. Chan,* R. G. Geyer†, J. E. Maslar,‡ and T. A. Vanderah*

*National Institute of Standards and Technology, *Materials Science and Engineering Laboratory Gaithersburg, Maryland 20899; †Electronics and Electrical Engineering Laboratory Boulder Colorado; and ‡Chemical Science and Technology Laboratory Gaithersburg, Maryland 20899*

Received May 23, 2000; in revised form August 18, 2000; accepted September 15, 2000; published online December 21, 2000

In the present work the effects of cation ordering on dielectric properties were isolated by investigating three polymorphs of $Ca(Ca_{1/3}Nb_{2/3})O_3$ that feature different arrangements of the Ca^{2+} and Nb^{5+} cations on the B-sites of the perovskite structure. Dielectric measurements at frequencies above 1 GHz revealed a systematic dependence of the properties on the type of cation ordering. In particular, the structure with 2:1 ordering exhibited a lower dielectric constant and a significantly more negative temperature coefficient of resonance frequency than the structures with 1:1 and newly described $\mathbf{k} = \frac{1}{4}[1\,1\,1]^*_c$ ordering. Rietveld refinements of structural models for the three $Ca_4Nb_2O_9$ polymorphs were conducted using X-ray and neutron powder diffraction data to elucidate structural details that could be correlated with the changes in dielectic properties. In all three polymorphs the cation ordering was combined with the same $b^-b^-c^+$ octahedral tilt system, and the structural refinements yielded similar magnitudes of the tilting angles. The most significant crystal-chemical difference between the three polymorphs was in the coordination environment of Nb^{5+}. Analysis of the refined bond distances indicated increasing average distortion of the Nb nearest-neighbor environment in going from the 1:1 to the $\mathbf{k} = \frac{1}{4}[1\,1\,1]^*_c$ to the 2:1 ordered structure. The increased fraction of strongly compressed Nb–O bonds in the 2:1 structure associated with the large distortion was correlated with the decrease in dielectic constant and more negative value of temperature coefficient of the resonant frequency obtained for this polymorph. Raman spectra obtained for the three polymorphs exhibited differences that were consistent with the observed structural chemistry.

Key Words: **perovskite; cation ordering; 1:1 ordering; 2:1 ordering; octahedral tilting; dielectric properties; microwave dielectrics; $Ca_4Nb_2O_9$; polymorphs; Rietveld refinement.**

INTRODUCTION

Complex perovskites with two or more cations mixed on the octahedrally coordinated B-sites are attractive candidates for use as dielectric resonators at microwave frequencies. These applications require a combination of high relative permittivity (ε), low dielectric loss ($\tan\delta$), and zero temperature coefficient of the resonant frequency (τ_f). For example, $BaMTa_2O_9$ ($M = Zn, Mg$) compounds, which exhibit uniquely low dielectric loss and are currently in commercial use, crystallize in a perovskite-like $AB'_{1/3}B''_{2/3}O_3$ structure with B′ (Zn^{2+} or Mg^{2+}) and B″ (Ta^{5+}) cations ordered on the B-sites (1–3). The type and degree of cation ordering are known to strongly affect the dielectric properties of complex perovskites (4, 5); however, the origin of this dependence is not well understood.

The effects of cation ordering on dielectric properties can be isolated by considering compounds that exhibit polymorphism: structures with different cation arrangements but the same chemical composition can then be obtained by varying the heat treatment. The existence of such polymorphs with distinctly ordered cation arrangements on the B-sites has been reported for $Ca_4Nb_2O_9$ ($= Ca(Ca_{1/3}Nb_{2/3})O_3$) (6, 7). The reported polymorphs include a high-temperature phase, quenchable from $T > 1400°C$, and two low-temperature phases that form below $T = 1400°C$. Levin *et al.* (7) proposed that in all three polymorphs, cation ordering of Ca and Nb cations on the B-sites is combined with the same octahedral tilting; the tilting system was described as $b^-b^-c^+$ according to the Glazer's notation (8). The high-temperature form exhibits 1:1 (NaCl-type) cation ordering (ordering vector $\mathbf{k} = \frac{1}{2}[1\,1\,1]^*_c$) and was described by a monoclinic $P2_1/c$ (14) structure with lattice parameters related to that of cubic perovskite according to $\sqrt{2}\,a_c \times \sqrt{2}\,a_c \times \sqrt{6}\,a_c$ (a_c refers to cubic perovskite), with $\beta \approx 125°$. This type of ordering in $A(B'_{1/3}B''_{2/3})O_3$ compounds results in a partially ordered structure with alternating $\{1\,1\,1\}_c$ planes occupied exclusively by B″ cations and a random mixture of B′ and the remaining B″ cations (4, 5). In the absence of octahedral tilting, 1:1 ordering creates a cubic superstructure with $Fm\bar{3}m$ symmetry and lattice parameter $a = 2a_c$. The low-temperature forms of $Ca_4Nb_2O_9$ were described by $P1$ (1) triclinic and $P2_1/c$ (14) monoclinic structures with lattice parameters, $\sqrt{6}\,a_c \times \sqrt{2}\,a_c \times 2\sqrt{2}\,a_c$ $\alpha \approx \gamma \approx 90°$, $\beta \approx 125°$, and $\sqrt{6}\,a_c \times \sqrt{2}\,a_c \times 3\sqrt{2}\,a_c$, $\beta \approx 125°$, respectively. The

0022-4596/01 $35.00

$P1$ structure exhibited ordering of Ca and Nb cations on the B-sites with the ordering vector $\mathbf{k} = \frac{1}{4}[1\,1\,1]^*_c$. Possible arrangements of the B-cations in this structure, hereafter denoted as $\mathbf{LT}_{1/4}$ [7], were proposed from the qualitative analysis of observed intensities in electron and X-ray powder diffraction patterns; however, the exact distribution of cations was not determined. The $\mathbf{LT}_{1/4}$ polymorph evolves from the 1:1 ordered phase on cooling below 1400°C, but is metastable and transforms upon further heating at $T < 1400$°C to the stable $P2_1/c$ phase with 2:1 ordering of Ca and Nb cations. The 2:1 ordering pattern (ordering vector $\mathbf{k} = \frac{1}{3}[1\,1\,1]^*_c$) corresponds to Ca (B′) and Nb (B″) ions arranged on $\{1\,1\,1\}_c$ planes with the sequence $\{B'B''B''\}$ (2). In the absence of octahedral tilting, this ordering results in a trigonal $P\bar{3}m1$ structure. Both 1:1 and 2:1 B-cation arrangements were observed in the commercial $Ba(Zn_{1/3}Ta_{2/3})O_3$–$BaZrO_3$ system (4); however, the $\mathbf{k} = \frac{1}{4}[1\,1\,1]^*_c$ ordering has not been reported. The present study was carried out to elucidate the effects of structural changes caused by changes in the type of cation ordering on dielectic properties of $Ca(Ca_{1/3}Nb_{2/3})O_3$.

EXPERIMENTAL

The specimens were synthesized by solid state reaction in air of $CaCO_3$ (99.95%) and optical grade Nb_2O_5. Before each heating, mixtures were ground 15–20 min using an agate mortar and pestle; the initial grinding was carried out as an ethanol slurry. Mixtures were pressed into pellets and placed on beds of sacrificial powder of the same composition on Pt foil supported in alumina combustion boats. After an initial overnight calcine at 1000°C reactions were completed by multiple heatings at 1375–1425°C until no further changes were observed in the X-ray powder diffraction patterns. Final heat-treatments were carried out at various temperatures to obtain the three $Ca_4Nb_2O_9$ polymorphs.

Samples were initially characterized by X-ray powder diffraction (XRPD) using an automated diffractometer equipped with incident Soller slits, theta compensating slits, a 0.2-mm receiving slit, a graphite monochromator, and a scintillation detector. Data were collected at ambient temperature using CuK_α radiation with a 0.02° (2θ) step size and a 2-s count time. Phase composition of the specimens was additionally verified by transmission electron microscopy (TEM) as described in (7).

X-ray powder diffraction data for Rietveld analysis were collected on a Siemens D500 diffractometer equipped with a focusing Ge incident beam monochromator, sample spinner, and a scanning position-sensitive detector (PSD). Copper $K\alpha_1$ radiation was used. The scan range was from 10° to 155° (2θ). The data collection time was 5 h; however, the PSD offers a counting rate roughly an order of magnitude greater than conventional detectors. Neutron powder diffraction data were collected under ambient conditions using the BT-1 32 detector neutron powder diffractometer at the NIST Center for Neutron Research reactor, NBSR. A Cu(3 1 1) monochromator with a 90° takeoff angle, $\lambda = 1.5404(2)$ Å, and in-pile collimation of 15 min of arc were used. The samples for neutron powder diffraction were loaded in vanadium can containers. Data were collected over the range of 3–165° 2θ with a step size of 0.05°. The GSAS (10) package was used for Rietveld structural refinement.

Previously we found that the high-temperature 1:1 ordered structure *was not* completely quenchable and that the specimens always contained nanodomains of the $\mathbf{LT}_{1/4}$ polymorph (7). These domains give rise to diffuse superlattice reflections at $\mathbf{k} = \frac{1}{4}[1\,1\,1]^*_c$ in electron diffraction patterns (7); however, these superlattice reflections were too weak to be detected by conventional X-ray powder diffraction. Subsequent annealing of quenched specimens at 1000°C resulted in growth of the $\mathbf{LT}_{1/4}$ domains as indicated by the appearance of broad superlattice reflection at $2\theta \approx 9°$. Numerous annealing experiments were carried out to determine the conditions necessary to grow the $\mathbf{LT}_{1/4}$ domains sufficiently large to eliminate extra broadening of superlattice reflections without nucleation of the stable 2:1 ordered phase, but these attempts were not successful. Rietveld refinement using powder diffraction data containing broad superlattice reflections was not feasible considering the combination of a large unit cell (~ 500 Å^3) and low symmetry ($P1$) for the $\mathbf{LT}_{1/4}$ structure. Refinement using a two-phase ($\mathbf{LT}_{1/4}$ plus 2:1) mixture model was also rejected due to significant overlap of the fundamental reflections of both phases. Instead, the refinement was conducted using data collected from a slightly off-stoichiometric specimen: at the molar composition $0.79CaO{:}0.21Nb_2O_5$ (1 mol% richer in Nb_2O_5) the $\mathbf{LT}_{1/4}$ structure was found to be stable in the temperature range 1400–1550°C (9). Phase-pure specimens of the $\mathbf{LT}_{1/4}$ phase with large domains were obtained at this composition by water quenching from 1525°C.

Dielectric properties were measured using cylindrical pellets with diameters and heights of approximately 8 and 4 mm, respectively. The details of the final heat treatments used to obtain specimens for dielectric measurements are given in Table 1. Microwave measurements were performed using the specimens as dielectric resonators in either a parallel plate waveguide or cylindrical cavity. Complex permittivity was measured at four temperatures (ambient, 50°, 75°, and 100°C) at frequencies near 9 GHz. Permittivity was calculated from the measured frequency of the TE_{011} resonance mode and sample dimensions. Variable-temperature and variable-frequency conductor losses were measured and accounted for in evaluation of dielectric loss tangents. The temperature coefficient of the resonant frequency (τ_f) was calculated from a linear regression analysis of the data obtained at different temperatures. Bulk densities were

TABLE 1
Final Heat Treatments for the Sintered $Ca_4Nb_2O_9$ Pellets Used for Dielectric Measurements

Phase composition	Heat treatment
1:1 Ordering[a]	1600°C/23 h AQ[b]
2:1 Ordering	1600°C 23 h, AQ + 1300°C/24h FC[c]
$\mathbf{LT}_{1/4}$	1600°C/23 h, AQ + 1000/20 min, AQ

[a] The 1:1 ordered phase was not completely quenchable and, according to transmission electron microscopy, the specimen contained nanodomains of the $\mathbf{LT}_{1/4}$ phase. The superlattice reflections due to $\mathbf{LT}_{1/4}$ nanodomains were too weak to be detected by conventional X-ray powder diffraction.

[b] AQ; air quench. The pellets could not be water quenched due to the lack of suitable sealed containers and thermal shock effects.

[c] FC; furnace cooled (over ~ 30 min) to 700°C followed by air quenching.

TABLE 2
Chemical Compositions and Schedule of Final Heat Treatments for the Powder Specimens Used for Rietveld Structural Analyses

Refined model	Chemical composition	heat treatment
1:1[a]	$Ca_4Nb_2O_9$ (80% CaO :20%Nb_2O_5)	1600°C/24 h, WQ[b]
2:1	$Ca_4Nb_2O_9$ (80%CaO: 20%Nb_2O_5)	1600°C/24 h, FC[c] + 1300°C/72 h, FC
$\mathbf{LT}_{1/4}$	$Ca_{3.864}Nb_{2.054}O_9$ (79%CaO:21%Nb_2O_5)	1525°C/72 h, WQ

[a] The 1:1 ordered phase was not completely quenchable and, according to transmission electron microscopy, the specimen contained nanodomains of the $\mathbf{LT}_{1/4}$ phase. The superlattice reflections due to $\mathbf{LT}_{1/4}$ nanodomains were too weak to be detected by conventional X-ray powder diffraction.

[b] WC, water quench.

[c] FC, furnace cooled (over ~ 30 min) to 700°C followed by air quenching.

calculated from specimen weights and dimensions, and the measured permittivity and dielectric loss were corrected for porosity using a two-phase media formalism (11). The precision of the measured properties was estimated from the measurements on three different specimens. The uncertainties in the reported permittivity and dielectric loss values were 4 and 3%, respectively, and are dominated by the uncertainties in the estimate of bulk densities (2%).

Raman spectra were obtained in a near-backscattering geometry with 514.5-nm radiation from an argon ion laser, appropriate holographic filters, a 0.46-m imaging spectrograph, and a back-illuminated, liquid-nitrogen-cooled, charge-coupled-device camera. The bandwidth was ca. 5 cm^{-1} and the instrumental reproducibility was $\pm$ 2 cm^{-1}. The power density at the sample was less than 3 W/cm^2.

RESULTS

1. Structural Analysis of the $Ca_4Nb_2O_9$ Polymorphs

The details of the final heat-treatments used to obtain specimens with different types of cation ordering for structural refinements are given in Table 2.

1:1 Ordered structure. The results of structural refinement of the 1:1 ordered phase in the quenched specimens using X-ray powder diffraction data were reported previously (7). In the present work, the 1:1 ordered model was refined using neutron powder diffraction data to obtain more accurate oxygen positional parameters. The structure was refined in the monoclinic space group $P2_1/c$ (14) with lattice parameters $a = 5.56133(3)$ Å ($\approx\sqrt{2}a_c$), $b = 5.76733(3)$ Å ($\approx\sqrt{2}a_c$), $c = 9.74629(9)$ Å ($\approx\sqrt{6}a_c$), and $\beta = 124.81°$ (X-ray powder diffraction data). Although as described previously, the high-temperature 1:1 ordered polymorph of $Ca_4Nb_2O_9$ was not completely quenchable, the $\mathbf{k} = \frac{1}{4}[111]^*_c$ ordered nanodomains did not produce *any* detectable features in X-ray or neutron diffraction patterns, and therefore their presence was omitted in the refinement. The refined model represents the *average* structure of the quenched specimen with an *approximate* 1:1 ordering of B-cations. The experimental and fitted profiles for this structure are shown in Fig. 1 and the results of the refinement, the atomic positions, and selected bond distances are summarized in Tables 3–5. Relatively large values of the refined isotropic temperature factors may reflect the effect of the $\mathbf{LT}_{1/4}$ nanodomains on the diffracted intensities. The oxygen displacements from the ideal cubic perovskite positions can be approximated by a $b^-b^-c^+$ octahedral tilting similar to that observed for $CaTiO_3$ (12). The c^+ and b^-b^- tilting angles of the $(Ca_{2/3}Nb_{1/3})O_6$ octahedra calculated from the refined B–O bond distances and lattice parameters (13) were 13′ and 17′, respectively. The corresponding tilting angles for the $[NbO_6]$ octahedra were 14′ and 18′, respectively. As seen from the R_{max}/R_{min} values in Table 5, both B-site octahedra are only slightly distorted. The average (Ca, Nb)–O distance (2.188 Å) is significantly larger than that for Nb1–O bonds (2.005 Å), as expected from the difference between the six-coordinated radii of Ca^{2+} and Nb^{5+} (1.00 and 0.64 Å, respectively (14)). The Ca cations on A-sites are eight coordinated with the bond valence sum (BVS) equal to 1.88. The first coordination sphere of the A-cation was defined to include all nearest-neighbor oxygen ions closer than the next nearest-neighbor B-cations.

2:1 Ordered structure. The 2:1 ordered structure was refined in the space group $P2_1/c$ (14) with lattice parameters $a = 9.81342(9)$ Å ($\approx\sqrt{6}\,a_c$), $b = 5.53495(5)$ Å ($\approx\sqrt{2}a_c$), $c = 17.34466(16)$ Å ($\approx 3\sqrt{2}a_c$), and $\beta = 125.4958(6)°$ (X-ray

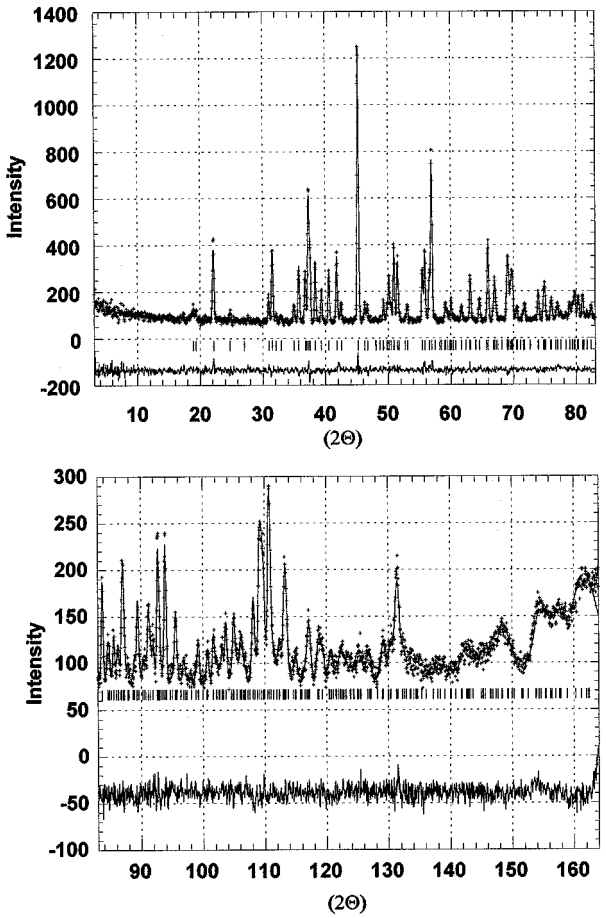

FIG. 1. Experimental (crosses) and calculated (line) neutron diffraction profiles for the 1:1 ordered polymorph of $Ca_4Nb_2O_9$. The refinement parameters are given in Table 3.

TABLE 3
Experimental Parameters for Neutron Powder Diffraction Studies of 1:1 Ordered $Ca_4Nb_2O_9$

Unit cell	$a = 5.5613(2)$ Å
(space group $P2_1/c$, No. 14)	$b = 5.7647(2)$ Å
	$c = 9.7448(5)$ Å
	$\beta = 124.794(4)^\circ$
	Volume = 255.56(2) Å^3
R_p (profile)	0.0582
R_{wp} (weighted profile)	0.0715
R_F^2 (Bragg)	0.0729
Reduced χ^2	1.025
Total refined variables	43
Minimum 2θ	3
Maximum 2θ	165
Number of reflections	593
Profile function	Pseudo-Voight (GSAS type 3)
Gaussian U, V, W	287, −241, 135
Cauchy X, Y	1.46, 5.40
Background function	Chebyschev polynomial (16 coefficients)

powder diffraction data). The volume per $\sqrt{6}\,a_c \times \sqrt{2}\,a_c \times \sqrt{2}\,a_c$, $\beta \approx 125^\circ$ unit cell in the 2:1 structure is 0.31% smaller than that of the 1:1 ordered structure. The initial atomic positions corresponded to those in the ideal cubic perovskite arrangement with 2:1 ordered B-cations. The experimental and fitted profiles for this structure are shown in Fig. 2, and the refinement parameters, atomic positions, and selected bond distances are summarized in Tables 6–8. The resulting structure can be described by a combination of a $b^-b^-c^+$ octahedral tilting system and 2:1 ordering of the B-cations, in agreement with the model proposed from the TEM data (7). Both of the crystallographically distinct $[NbO_6]$ octahedra, which are vertex-linked simultaneously to $[CaO_6]$ and other $[NbO_6]$ octahedra, are significantly distorted, as seen from the R_{max}/R_{min} values in Table 8. In contrast, the $[CaO_6]$ octahedra, which are connected exclusively to $[NbO_6]$ octahedra remain relatively regular. The BVS calculations (15) indicate a large compressive bond strain about the Ca cations occupying B-sites, while the bonding about Nb is in tension. The Nb cations are displaced from the centers of octahedra toward oxygens shared by other B-site Ca cations. The resulting Nb–O bond distances (~ 1.9 Å) in Nb–O–Ca linkages are significantly shorter than those in Nb–O–Nb linkages (~ 2.1 Å); however, the average Nb–O bond length (~ 2 Å) remains approximately the same as in the 1:1 ordered structure. The angles of the b^-b^- and c^+ octahedral rotations for the $[CaO_6]$ octahedra, determined using the appropriate structural projections, were 17° and 11°, respectively; the c^+ tilting angle (11°) is slightly smaller than that (13°) for the $[(Ca_{2/3}Nb_{1/3})O_6]$ octahedron in the 1:1 ordered structure. Similar (within 1°) tilting angles were obtained for the $[NbO_6]$ octahedra, although determination was somewhat ambiguous due to significant distortion of the $[NbO_6]$

TABLE 4
Refined Structural Parameters for the 1:1 Ordered $Ca_4Nb_2O_9$ (from Neutron Powder Diffraction Data)

Atom	Site	x	y	z	Occupancy	$U\times100$ Å^2
Ca	4e	0.2396(14)	0.0526(4)	0.2506(12)	1	1.58(7)
Nb1	2c	0	0.5	0	1	0.91(12)
Nb2/Ca	2b	0.5	0	0	0.33/0.67	1.11(16)
O1	4e	0.6561(10)	0.9555(5)	0.2613(8)	1	1.97(4)[a]
O2	4e	0.1226(11)	0.2108(7)	0.9370(6)	1	1.97(4)
O3	4e	0.7534(10)	0.3153(7)	0.0469(6)	1	1.97(4)

Note. Lattice parameters: $a = 5.5613(2)$ Å, $b = 5.7647(2)$ Å, $c = 9.7448(5)$ Å, $\beta = 124.794(4)^\circ$; space group $P2_1/c$ (14).

[a] Temperature factors of the oxygen ions were constrained to be equal.

TABLE 5

Bond Distances (Å), Average Bond Distance (Å), Site Distortion Ratio, and Bond Valence Sum (BVS, v.u.) about Each of the Cation Sites in the 1:1 Ordered $Ca_4Nb_2O_9$ Structure

		B sites		
	Nb1–O1	2.0113 (3) × 2	Ca/Nb–O1	2.1891 (3) × 2
	–O2	2.0211 (1) × 2	–O2	2.1865 (1) × 2
	–O3	1.9825 (1) × 2	–O3	2.1889 (1) × 2
Average		2.005		2.188
R_{max}/R_{min}		1.019		1.001
BVS_{obs} [a]		4.66		3.16
BVS_{calc}		5.00		3.00
		A site[b]		
	Ca–O1	2.327 (4)	–O3	2.274 (7)
	–O1	2.415 (4)	–O3	2.771 (8)
	–O2	2.887 (9)	–O3	2.629 (7)
	–O2	2.355 (4)	–O3	2.373 (8)
Average		2.560		
BVS_{obs}		1.86		
BVS_{calc}		2.00		

[a] Observed bond valence sum values (BVS_{obs}) were calculated from experimentally determined bond distances using the formalism and parameters of Brown and Altermatt (15); calculated BVS values were obtained from the formal valences and presumed occupancies of Ca^{2+} and Nb^{5+} in 1:1 ordered $Ca_4Nb_2O_9$ (= $Ca[(Ca_{2/3}Nb_{1/3})(Nb)]O_3$).

[b] The first coordination sphere of the A-cation was defined to include only those oxygen nearest neighbors which are closer to the A-cation than the next nearest-neighbor B-cation.

units. The BVS values observed for the A-site Ca ions are similar to those in the 1:1 ordered structure.

$LT_{1/4}$ structure. The initial model for the $\mathbf{LT}_{1/4}$ ordered phase was derived from qualitative analyses of the X-ray powder diffraction and TEM data (7). Comparison of the X-ray diffraction patterns from quenched specimens with those subsequently annealed at 1000°C and 1100°C indicated that both the intensity and width of the $(1\,0\,1)_0$[1] ($2\theta \approx 19°$, Fig. 3) reflection at $\mathbf{k} = \frac{1}{2}[1\,1\,1]^*_c$ are approximately unaffected by the $1:1 \rightarrow \mathbf{LT}_{1/4}$ transition. The structure factor of this reflection in the 1:1 ordered structure is determined primarily by the difference in composition $\Delta c = c_1 - c_2$ of the alternating $\{1\,1\,1\}_c$ cation planes (Fig. 4a). Since these reflections remain nearly unaffected by the $1:1 \rightarrow \mathbf{LT}_{1/4}$ transition, the difference $\Delta c = \{(c_1 + c_{1'}) - (c_2 + c_{2'})\}$, where c_1, $c_{1'}$, c_2, $c_{2'}$ are the compositions of the corresponding cation $\{1\,1\,1\}_c$ planes in the $\mathbf{LT}_{1/4}$ unit cell (Fig. 4b), must be preserved in the structural model. This condition is satisfied if planes **2** and **2′** (Fig. 4b) remain occupied predominantly by Nb, and the transition primarily involves redistribution of Ca and Nb cations between planes **1** and **1′** occupied by the disordered Ca/Nb mixture in the 1:1 ordered structure. Accordingly, Ca segregates to one of these two planes (say plane **1**), while the other plane (**1′**) is still occupied by a disordered mixture of Nb and the remaining Ca ions. The proposed model is illustrated schematically in Fig. 4b, using different shades for chemically distinct octahedra. Such B-cation distribution is also consistent with pseudoextinctions of some of the $\mathbf{LT}_{1/4}$ superlattice reflections observed in the electron microdiffraction patterns from single domains of the $\mathbf{LT}_{1/4}$ polymorph (7).

Refinement of the $\mathbf{LT}_{1/4}$ ordered structure was conducted using combined X-ray and neutron powder diffraction data. The initial atomic positions corresponded to those in an undistorted perovskite structure with B-sites ordered as described above. The $\mathbf{LT}_{1/4}$ structure was assumed to contain Ca vacancies on the A-sites corresponding to the specimen's 79% CaO:21% Nb_2O_5 stoichiometry, while the B sites were assumed to be fully occupied. Soft constraints were imposed on the total Ca/Nb ratio. The occupancies of

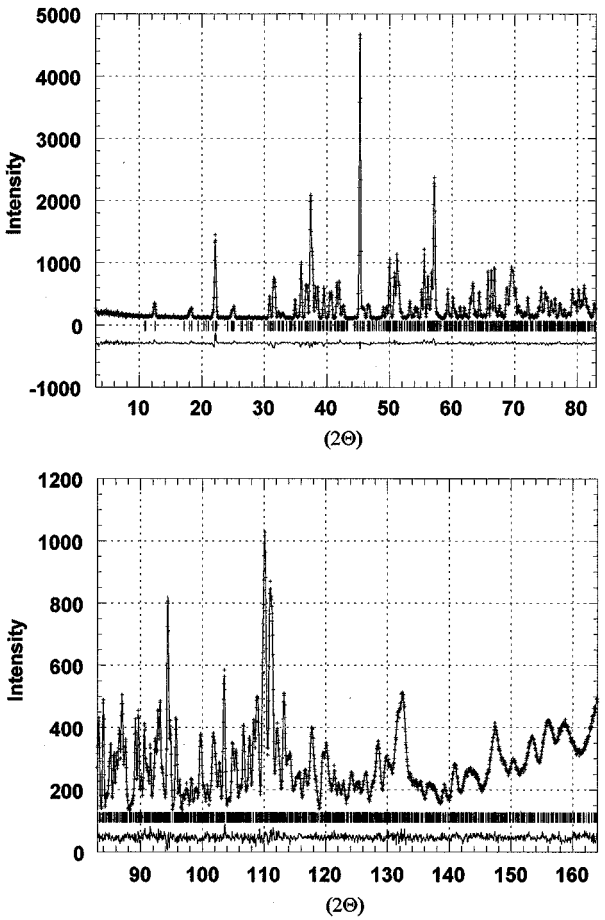

FIG. 2. Experimental (crosses) and calculated (line) neutron diffraction profiles for the 2:1 ordered polymorph of $Ca_4Nb_2O_9$. The refinement parameters are given in Table 6.

[1] Subscript "o" refers to the pseudoorthorhombic $\sqrt{2}a_c \times \sqrt{2}a_c \times 2a_c$ (space group No. 14 $P2_1/n$, nonstandard setting of axes) units cell of the 1:1 ordered $Ca_4Nb_2O_9$ polymorph.

TABLE 6
Experimental Parameters for Neutron Diffraction Studies of 2:1 Ordered $Ca_4Nb_2O_9$

Unit cell	$a = 9.81590(10)$ Å
(space group $P2_1/c$, 14)	$b = 5.53628(5)$ Å
	$c = 17.35016(16)$ Å
	$\beta = 125.501(1)^\circ$
	Volume = 767.60(1) Å^3
R_p (profile)	0.0296
R_{wp} (weighted profile)	0.036
R_F^2 (Bragg)	0.0229
Reduced χ^2	1.269
Total refined variables	79
Minimum 2θ	3
Maximum 2θ	165
No. of reflections	1743
Profile function	Pseudo-Voight (GSAS type 3)
Gaussian U, V, W	221, −247, 148
Cauchy X, Y	0.27, 1.51
Background function	Chebyschev polynomial (12 coefficients)

the B-sites were initially derived using X-ray powder diffraction data to obtain the best fit for those superlattice reflections whose structure factors depend primarily on the cation distribution (Fig. 5). Introducing a partial disorder on the B-sites was necessary to obtain positive isotropic temperature factors for the cations on these positions. At this point, a few cation distributions *alternative*[2] to the model in Fig. 4b were tested, but none resulted in a satisfactory fit to the experimental data. During subsequent refinement, restraints were imposed on the B–O bond distances to keep them chemically reasonable. The restraints were estimated according to the chemical composition of specific B-sites, and assuming $R_{Ca-O} = 2.3$ Å and $R_{Nb-O} = 2.0$ Å bond distances for the sites fully occupied by Ca and Nb cations, respectively. The weight of the restraints was decreased progressively as the refinement proceeded and their contribution to the sum of weighted squared differences in the final cycle of the refinement was 1.5%. The neutron and X-ray powder diffraction experimental and fitted patterns are represented in Figs. 6a and 6b, respectively, and the experimental parameters, refinement results, and selected bond distances are summarized in Tables 9–11.

Results of the refinement demonstrate that the proposed structural model (Fig. 4b) provides a satisfactory description of the both neutron and X-ray powder diffraction data obtained for the $\mathbf{k} = \frac{1}{4}[1\,1\,1]_c^*$ ordered phase. The displacements of oxygen atoms from ideal perovskite positions indeed can be approximated by $b^-b^-c^+$ tilting of the $[BO_6]$ octahedra (Fig. 7), as proposed from crystallographic analysis of the TEM data (7). Moreover, orientational relation-

TABLE 7
Refined Structural Parameters from Neutron Powder Diffraction Data for the 2:1 Ordered $Ca_4Nb_2O_9$

Atom	Site	x	y	z	$U \times 100$ Å^2
Ca1	2a	0	0	0	1.11(7)
Ca2	2d	0.5	0.5	0	1.11(7)
Nb1	4e	−0.0018(3)	0.0095(6)	0.3367(2)	0.48(3)
Nb2	4e	0.4937(3)	0.0093(5)	0.1631(2)	0.48(3)
O1	4e	−0.0418(4)	0.2125(5)	0.0968(2)	0.96(6)
O2	4e	0.4566(4)	0.7119(6)	0.2182(2)	0.99(8)
O3	4e	0.0450(4)	0.8021(6)	0.2495(2)	0.88(7)
O4	4e	0.5578(4)	0.2950(6)	0.1280(2)	0.90(8)
O5	4e	0.0789(4)	0.6806(6)	0.1004(2)	1.12(8)
O6	4e	0.4356(4)	0.8306(6)	0.0527(2)	1.17(6)
O7	4e	0.2542(4)	0.4114(5)	0.2648(2)	0.89(7)
O8	4e	0.7733(4)	0.6144(5)	0.0762(2)	0.91(6)
O9	4e	0.2694(4)	0.1132(5)	0.1056(2)	1.01(7)
Ca3	4e	0.2671(5)	0.5182(8)	0.0737(3)	1.42(8)
Ca4	4e	0.7535(6)	0.4978(8)	0.2691(3)	1.17(8)
Ca5	4e	0.7596(5)	0.0164(8)	0.1069(2)	1.37(8)

Note. All sites were assumed to be fully occupied. Temperature factors of the cations occupying B-sites were grouped by the atom type. Lattice parameters $a = 9.81590(10)$ Å, $b = 5.53628(5)$, $c = 17.35016(16)$ Å, $\beta = 125.501(1)^\circ$, space group $P2_1/c$ (14).

TABLE 8
Bond Distances (Å), average Bond Distance (Å), Site Distortion Ratio (R_{max}/R_{min}) and Bond Valence Sum (BVS, v.u.) about Each of the Cation Sites in the 2:1 Ordered $Ca_4Nb_2O_9$ Structure

B Sites							
Ca1–O1	2.274 (3) × 2	Ca2–O4	2.253 (3) × 2	Nb1–O1	1.909 (4)	Nb2–O2	2.040(5)
–O5	2.279 (3) × 2	–O6	2.293 (3) × 2	–O3	2.151 (4)	–O2	2.138 (5)
–O9	2.261 (3) × 2	–O8	2.286 (3) × 2	–O3	2.075 (5)	–O4	1.927 (5)
				–O5	1.903 (4)	–O6	1.925 (4)
				–O7	2.114 (5)	–O7	2.095 (4)
				–O8	1.928 (4)	–O9	1.904 (4)
Average	2.271		2.277		2.013		2.004
R_{max}/R_{min}	1.008		1.018		1.130		1.120
BVS_{obs}	2.64		2.60		4.73		4.80
BVS_{calc}	2.00		2.00		5.00		5.00
A Sites							
Ca3–O1	2.875 (5)	Ca4–O1	2.681 (6)	Ca5–O1	2.326 (6)		
–O2	2.341 (5)	–O2	2.772 (5)	–O3	2.707 (5)		
–O4	2.726 (5)	–O2	2.709 (5)	–O3	2.615 (5)		
–O5	2.330 (5)	–O3	2.435 (5)	–O4	2.698 (5)		
–O5	3.155 (5)	–O4	2.342 (5)	–O6	2.929 (5)		
–O6	2.561 (5)	–O5	2.568 (5)	–O6	2.428 (5)		
–O8	2.502 (5)	–O7	2.354 (5)	–O7	2.379 (5)		
–O9	2.306 (5)	–O9	2.399 (5)	–O8	2.311 (5)		
Average	2.601		2.533		2.549		
BVS_{obs}	1.83		1.90		1.91		
BVS_{calc}	2.00		2.00		2.00		

[2] For example, a model with {CaNbNb(Ca/Nb)...} sequence of the {1 1 1} cation layers, or a model with Ca and Nb located in the same {1 1 1} layer.

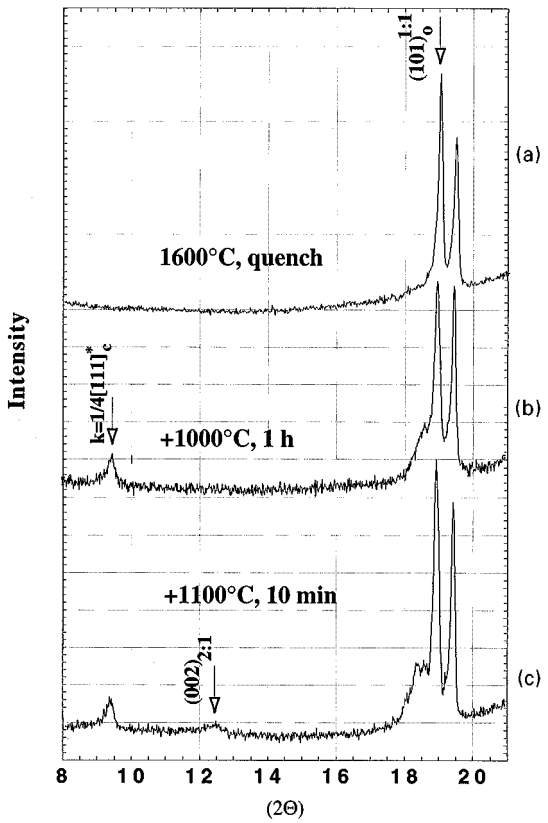

FIG. 3. Low-angle portions of X-ray powder diffraction patterns from the $Ca_4Nb_2O_9$ specimens quenched from (a) 1600°C and subsequently annealed at (b) 1000°C (1 h) and (c) 1100°C (10 min). The superlattice reflection at $\sim 9°$ belongs to the $\mathbf{LT}_{1/4}$ structure. Note the appearance of the (0 0 2) reflection (near 12.5°) of the 2:1 ordered phase in the specimen annealed at 1100°C. The strong $(1\,0\,1)_0$ reflection is primarily due to 1:1 ordering of Ca and Nb cations. The figure demonstrates that both the intensity and the width of this reflection remains approximately unaffected by the 1:1 → $\mathbf{LT}_{1/4}$ transition; this observation was used to derive a structural model for the $\mathbf{LT}_{1/4}$ polymorph.

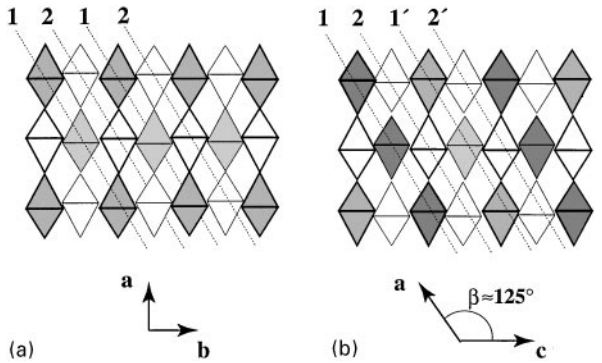

FIG. 4. Schematic projections of the (a) 1:1 ordered array, (b) proposed B-cation distribution in the $\mathbf{LT}_{1/4}$ polymorph. Chemically distinct B-site octahedra are indicated by shading; white, dark gray, and light gray shades refer to the B-sites occupied by Nb, Ca, and random Ca/Nb mixture, respectively.

ships between the directions of the tilting axes and the ordering vector $\mathbf{k} = \frac{1}{4}(1\,1\,1]^{*}_{c}$ matches the orientation relationship between the 1:1 ordered and $\mathbf{LT}_{1/4}$ phases determined by electron diffraction (7). Note that no assumption was made in the initial model about the displacements of oxygen ions. As seen from the R_{max}/R_{min} values in Table 11, distortion of the B-site octahedra occupied predominantly by Nb is intermediate between that in the 1:1 and 2:1 ordered structures.

Assuming full occupancy of planes **2** and **2′** by Nb in both 1:1 and $\mathbf{LT}_{1/4}$ structures (Fig. 4), the 1:1 → $\mathbf{LT}_{1/4}$ ordering reaction can be approximately described by the order parameter $\eta = 3(n_{Ca} - \frac{2}{3})$, where n_{Ca} is the Ca-occupancy of plane **1** in Fig. 4b. For the $Ca_4Nb_2O_9$ stoichiometry, a zero value of the order parameter corresponds to the 1:1 ($n_{Ca} = \frac{2}{3}$) ordered structure, while a value of unity describes $\mathbf{LT}_{1/4}$ phase. The intensity of the $\mathbf{k} = [0\,0\,1]^{*}_{LT_{1/4}} \approx 1/4[1\,1\,1]^{*}_{c}$ superlattice reflection is proportional to η^2. Thus, the 1:1 ordered structure indeed can be considered as an approximation of the $\mathbf{LT}_{1/4}$ structure with the order parameter η close to zero, as it was assumed in the analysis of the quenched specimens. Note that the 1:1 → $\mathbf{LT}_{1/4}$ transformation must be a first-order transition, as discussed in detail previously (7).

Dielectric Properties

The dielectric properties obtained for the specimens containing different polymorphs of $Ca_4Nb_2O_9$ are listed in Table 12. The change from either a 1:1 ordered or $\mathbf{LT}_{1/4}$

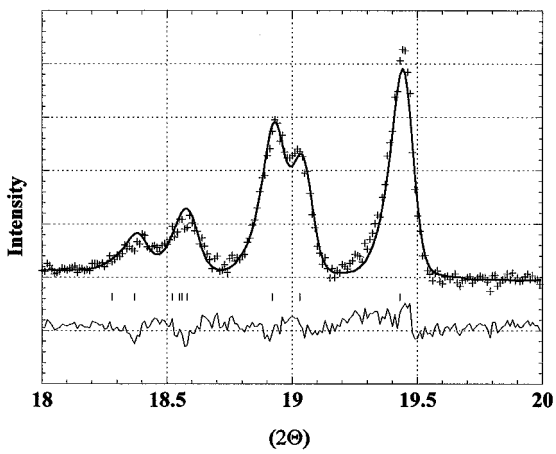

FIG. 5. Experimental (crosses) and calculated (line) profiles for the low-angle region of the X-ray powder diffraction pattern corresponding to the $\mathbf{LT}_{1/4}$ polymorph at composition $0.79CaO{:}0.21Nb_2O_5$. This part of the pattern contains the superlattice reflections predominantly sensitive to the distribution of Ca and Nb cations. Such superlattice reflections were used to obtain initial values of B-site occupancies.

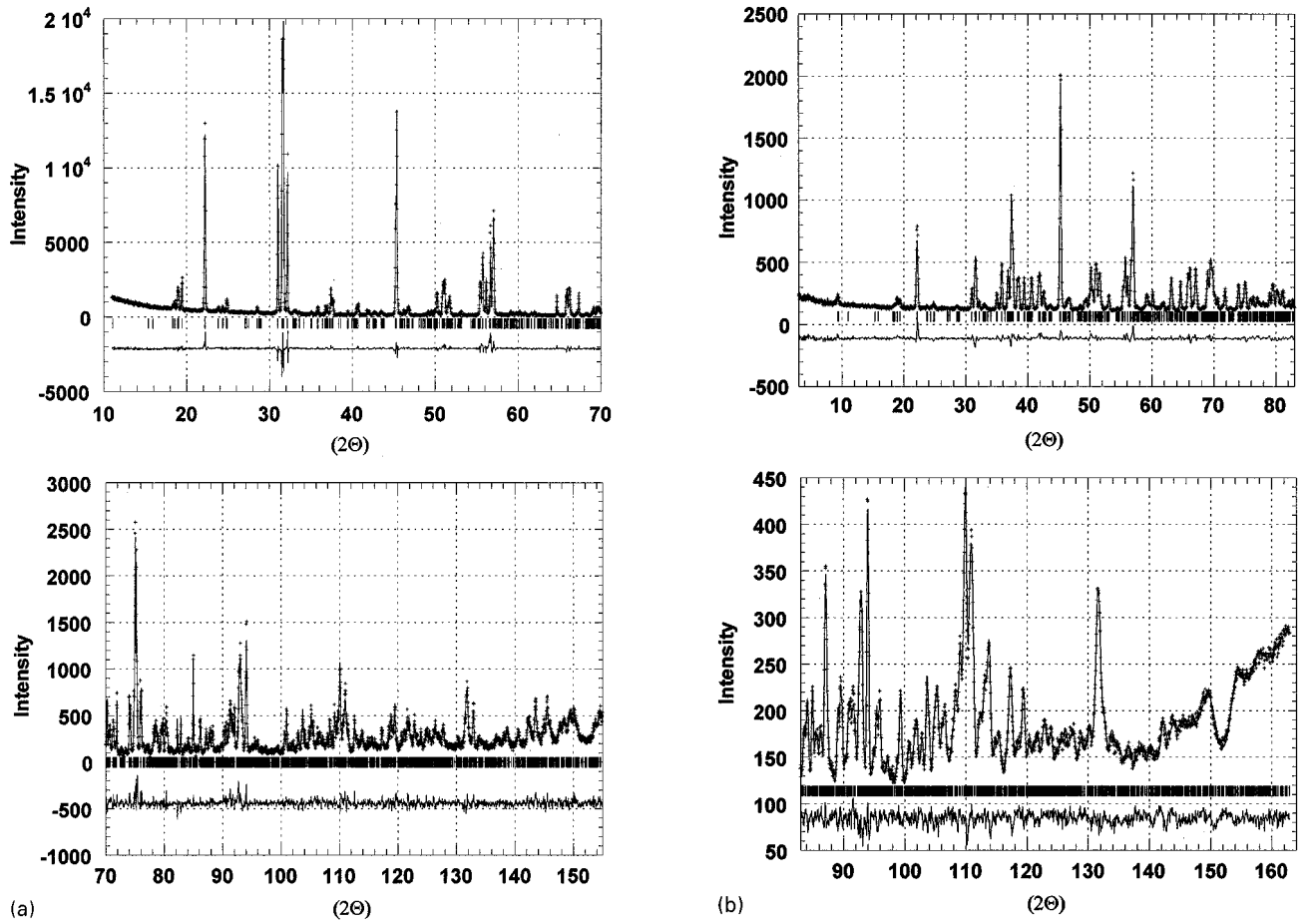

FIG. 6. Experimental (crosses) and calculated (line) X-ray (a) and neutron (b) powder diffraction profiles of the $\mathbf{LT}_{1/4}$ polymorph at composition $0.79CaO{:}0.21Nb_2O_5$.

phase to the 2:1 ordered polymorph is accompanied by a statistically significant decrease in permittivity. The temperature coefficient of the resonance frequency for the 2:1 ordered specimen is more negative and about 5 times larger in magnitude than the τ_f of either the 1:1 or $\mathbf{LT}_{1/4}$ specimens. The difference in dielectric permittivity of the 1:1 and $\mathbf{LT}_{1/4}$ specimens is within the estimated uncertainty. As seen in Table 12, the Qf product increases monotonically with the change in the type of cation ordering so that $Qf_{2:1} > Qf_{\mathrm{LT}\,1/4} > Qf_{(1:1\,+\,\mathrm{LT}\,1/4)}$.

Raman Spectroscopy

Raman spectra of powder samples, obtained by grinding portions of pellets containing different $Ca_4Nb_2O_9$ polymorphs are shown in Fig. 8. The spectra from both 1:1 and $\mathbf{LT}_{1/4}$ polymorphs are similar to each other (except for the peaks A_1 and A_2 in the spectrum of the $\mathbf{LT}_{1/4}$), but differ significantly from the spectrum of the 2:1 ordered polymorph. These results are consistent with the structural similarity of the 1:1 and $\mathbf{LT}_{1/4}$ polymorphs are their dissimilarity from the 2:1 ordered arrangement. Factor-group analysis for the $P2_1/c$ monoclinic structure with a combination of 1:1 ordering and $b^-b^-c^+$ octahedral tilting predicted 24 Raman active modes ($12\mathbf{A}_g + 12\mathbf{B}_g$), of which only 12 were detected in the present spectra. For the 2:1 ordered $P2_1/c$ monoclinic structure with $b^-b^-c^+$ tilting, 84 Raman active modes are expected ($42\mathbf{A}_g + 42\mathbf{B}_g$), while only 29 of these were experimentally observed. The spectra of all three polymorphs show strongest peak(s) at frequencies near $800\,cm^{-1}$, which is typical for complex perovskites with both 1:1 and 2:1 ordering of B-cations (16,17). For the 1:1 ordered structure with $Fm\bar{3}m$ symmetry, the $\sim 800\,cm^{-1}$ peak has been assigned to the A_{1g} mode associated with a simple "breathing" of the $[BO_6]$ octahedra; however, for the 2:1 ordered (untilted) $P\bar{3}m1$ structure, the ion motion associated with this mode is more complex (17, 18).

DISCUSSION

The present results establish a systematic dependence of the dielectric properties on the type of cation ordering: the

TABLE 9

Experimental Parameters and Refinement Results from Neutron and X-ray Powder Diffraction Studies of the $LT_{1/4}$ Polymorph at Composition $0.79CaO:0.21Nb_2O_5$

Unit cell	$a = 9.82099(7)$ Å	$\alpha = 90.1604(4)^\circ$
space group $P1$ (1)	$b = 5.55791(4)$ Å	$\beta = 125.543(1)^\circ$
	$c = 11.51803(9)$ Å	$\gamma = 89.9201(5)^\circ$
		Volume = 511.562(7) Å^3
	Neutron	X-ray
R_p (profile)	0.0333	0.0812
R_{wp} (weighted profile)	0.0409	0.1097
R_F^2 (Bragg)	0.0456	0.0619
Reduced χ^2	4.76	
No. of structural parameters	159	
Total No. of restraints	48	
Contribution of restraints to χ^2	1.5%	
Contribution to χ^2	8.9%	89.6%
Minimum 2θ	3	10
Maximum 2θ	165	155
No. of reflections	2320	2213
Profile function	Pseudo-Voight (GSAS type 3)	
Gaussian U, V, W	237, −231, 120	8.8, −10.1, 8.1
Cauchy X, Y	2.494, 2.794	0.651, 7.029
Background function	Chebyschev polynomial (12 coefficients)	GSAS type 6 (8 coefficients)

2:1 ordered phase exhibited lower permittivity, higher Qf product, and significantly more negative value of τ_f[3] than either the 1:1 or $\mathbf{LT}_{1/4}$ polymorphs. The observed dielectric properties of the $\mathbf{LT}_{1/4}$ phase are intermediate between those of the 1:1 and 2:1 ordered phase and are more similar to the former. The similarity in properties of the 1:1 and $\mathbf{LT}_{1/4}$ polymorphs is consistent with their closely related structures (Fig. 7) and similar Raman spectra. Unfortunately, the differences in properties of these two phases are obscured by the inability to completely quench the 1:1 ordered polymorph as a pure phase. The differences in ε and τ_f can be attributed exclusively to the differences in the type of cation arrangement, considering that all polymorphs have identical chemical composition and exhibit very similar octahedral tilting. The interpretation of differences of Qf, however, is ambiguous due to the possible contribution of extrinsic losses. A probable origin of such losses is the high density of different types of domain boundaries identified in the present specimens by TEM (7). The possible effects of post-quenching annealings on the improved dielectric losses of the $\mathbf{LT}_{1/4}$ and 2:1 specimens due to decreased conduction losses also cannot be ruled out, even though no change in color was observed after different heat treatments.

The observed changes in permittivity and temperature coefficient of the different $Ca_4Nb_2O_9$ polymorphs must be directly related to changes in restoring force constants and effective charges associated with certain polar phonons. Since the chemical composition does not vary, the differences in force constants may arise from differences in the distribution of bond distances, which were analyzed using the results of structural refinements. Following the discussion by Kunz and Brown (19), it was assumed that the

[3] Temperature coefficient of the resonance frequency (τ_f) is related to the temperature coefficient of permittivity (τ_ε) as $\tau_f = -\frac{\tau_\varepsilon}{2} - \alpha_l$, where α_l is the linear thermal expansion coefficient, which typically varies between 8 and 10 ppm/°C. Assuming $\alpha_l = 10$ ppm/°C, the τ_ε changes from −12 ppm/°C for the 1:1 ordered specimen to +60 ppm/°C for the 2:1 ordered polymorph.

TABLE 10

Structural Parameters for the $LT_{1/4}$ Structure from the Combined Refinement of Neutron and X-ray Powder Diffraction Data

Atom	Occupancy	x	y	z	$U\times100$ Å^2
O1	1	0.2421(31)	0.612(4)	0.2111(25)	
O2	1	0.0453(31)	0.343(5)	0.2963(26)	
O3	1	0.7421(32)	0.138(5)	0.2705(26)	
O4	1	0.9611(30)	0.815(5)	0.2018(25)	
O5	1	0.7798(33)	0.402(5)	0.5439(27)	
O6	1	0.5592(33)	0.749(5)	0.2476(31)	
O7	1	0.4183(31)	0.202(5)	0.2246(25)	
O8	1	0.9400(28)	0.691(5)	0.4688(25)	
O9	1	0.4655(33)	0.332(5)	0.5297(29)	
O10	1	0.7670(28)	0.413(4)	0.0267(23)	
O11	1	0.9506(31)	0.723(5)	0.9615(26)	
O12	1	0.4625(31)	0.322(4)	0.0094(25)	
O13	1	0.7583(25)	0.110(4)	0.7799(22)	
O14	1	0.9660(31)	0.823(5)	0.7109(25)	
O15	1	0.2553(30)	0.601(4)	0.7537(21)	1.3(1)
O16	1	0.056(33)	0.319(5)	0.8090(27)	
O17	1	0.2848(31)	−0.091(5)	0.4894(24)	
O18	1	0.4609(31)	0.205(5)	0.7568(27)	
O19	1	0.5576(31)	0.740(5)	0.7628(25)	
O20	1	0.0816(30)	0.229(5)	0.59187(23)	
O21	1	0.5898(33)	0.842(5)	0.5294(27)	
O22	1	0.2677(26)	−0.083(4)	−0.0053(23)	
O23	1	0.0606(32)	0.241(5)	0.0551(24)	
O24	1	0.5452(28)	0.840(5)	0.0004(24)	
Ca25	0.972(4)	0.2377(25)	0.0468(15)	0.2751(22)	
Ca26	0.972(4)	0.7653(20)	0.5283(20)	0.2454(28)	
Ca27	0.972(4)	0.7674(22)	0.0137(25)	0.4924(28)	
Ca28	0.972(4)	0.2522(18)	0.5135(24)	0.0280(27)	
Ca29	0.972(4)	0.7455(27)	0.5340(30)	0.7276(23)	0.8(1)
Ca30	0.972(4)	0.2763(22)	0.0146(31)	0.7914(19)	
Ca31	0.972(4)	0.2677(22)	0.4934(23)	0.5531(25)	
Ca32	0.972(4)	0.7522(24)	0.0044(21)	0.739(22)	
(Ca/Nb)33	0.97(2)/0.03(2)	0.0136(17)	0.0153(30)	0.3976(10)	0.84(1)
(Ca/Nb)34	0.93/(2)0.07(2)	0.5117(25)	0.5135(36)	0.3822(20)	0.84(1)
(Ca/Nb)35	0.01(1)/0.99(1)	0.0111(9)	0.5175(18)	0.6383(7)	0.37(1)
(Ca/Nb)37	0.00(1)/1.00(1)	0.5117(9)	0.0288(18)	0.1390(8)	0.37(1)
(Ca/Nb)39	0.27(1)/0.73(1)	0.5147(12)	0.5170(20)	0.8840(10)	0.29(1)
(Ca/Nb)41	0.07(1)/0.93(1)	0.5084(9)	0.0210(15)	0.6247(7)	0.37(1)
(Ca/Nb)43	0.02(2)/0.98(2)	0.0129(9)	0.5270(17)	0.1392(8)	0.37(1)
(Ca/Nb)45	0.26(2)/0.74(2)	0.0117(11)	0.0185(20)	0.8889(9)	0.29(1)

Note. Lattice parameters $a = 9.82099(7)$ Å, $b = 5.55791(4)$ Å, $c = 11.51803(9)$ Å, $\alpha = 90.1604(4)^\circ$, $\beta = 125.543(1)^\circ$, $\gamma = 89.9201(5)^\circ$, space group $P1$ (1). The isotropic temperature parameters for the oxygen and Ca(A-site) atoms were constrained to be equal for the same atom type.

TABLE 11
B-site Metal–Oxygen Distances (Å) in the $LT_{1/4}$ Structure

	B sites							
	Ca**33**–O2	2.28	Ca**34**–O1	2.27	Nb**35**–O5	1.97	Nb**37**–O3	1.95
	–O3	2.28	–O5	2.26	–O8	1.91	–O6	1.88
	–O4	2.29	–O6	2.28	–O14	2.05	–O7	1.94
	–O8	2.27	–O7	2.28	–O15	2.01	–O12	2.07
	–O17	2.30	–O9	2.24	–O16	2.07	–O22	2.06
	–O20	2.26	–O21	2.30	–O20	1.94	–O24	2.09
Average		2.28		2.27		1.99		2.00
R_{max}/R_{min}		1.02		1.03		1.08		1.10
	Nb**41**–O9	1.96	Nb**43**–O1	1.95	Ca/Nb**39**–O10	2.12	Ca/Nb**45**–O11	2.09
	–O13	2.09	–O2	1.94	–O12	2.10	–O13	2.10
	–O17	1.91	–O4	1.94	–O15	2.13	–O14	2.12
	–O18	2.10	–O10	2.07	–O18	2.13	–O16	2.08
	–O19	2.09	–O11	2.07	–O19	2.09	–O22	2.14
	–O21	1.96	–O23	2.05	–O24	2.15	–O23	2.08
Average		2.02		2.00		2.12		2.100
R_{max}/R_{min}		1.09		1.07		1.03		1.03

Note. The standard uncertainties due to counting statistics were approximately 0.01 Å.

major crystal-chemical factors which determine the distortion of the B- and A-cation environments in the perovskite-like $A_3B'B''_2O_9$ structure include bond network asymmetry and lattice stresses; a possible effect of electronic distortion was not considered here. The reasons for the out-of-center distortion around the Me^{5+} cation are revealed by mapping the general $A_3B'B''_2O_9$ formula unit ($A = Me^{2+}$, $B' = Me^{2+}$, $B'' = Me^{5+}$) onto the bond graph corresponding to the 2:1 ordered perovskite-like arrangement (Fig. 9a). The bond valences predicted from the valence sum rule (19, 20),

$$\sum_j s_{ij} = V_i,$$

are indicated in the bond graph; here s_{ij} is a valence of the bond between atoms i and j, and V is the formal valence of atom i. Thus, to comply with the BVS requirements for the oxygen ions, half of the B″–O bonds must be compressed ($s = 1$ v.u.) while the other half are stretched ($s = \frac{2}{3}$ v.u.), as compared with the ideal B″–O bond valence of $\frac{5}{6}$. This can be realized by displacements of the B″-cations along the $\langle 1\,1\,1 \rangle_c$ direction toward the B′-occupied $\{1\,1\,1\}_c$ cation plane. Such displacements indeed have been observed in the $Ba(Mg_{1/3}Ta_{2/3})O_3$ structure (21), where bond valences calculated from the refined cation–oxygen bond distances ($s_{Mg-O1} = 0.33$ v.u., $s_{Ta-O1} = 0.99$ v.u., $s_{Ta-O2} = 0.65$ v.u.) are in good agreement with the predicted values. The directions of the Nb-displacements in the presently refined 2:1 ordered $Ca_4Nb_2O_9$ structure are also in good agreement with those predicted from the asymmetry of the bond network, and the bond valences observed for the Nb–O bonds in the Nb–O–Ca linkages match closely the predicted value of unity. The *average* out-of-center distortion of B″-cation environments can be effectively zeroed in the partially ordered structure adopting the NaCl-type arrangement (1:1 ordering) of the B-cations (Fig. 9b).

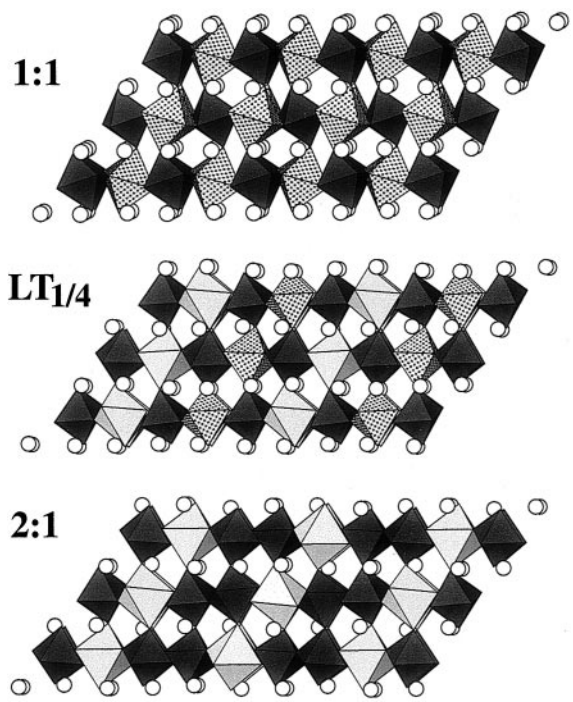

FIG. 7. Illustrations of the 1:1 (top), $\mathbf{LT}_{1/4}$ (middle), and 2:1 (bottom) ordered polymorphs of $Ca_4Nb_2O_9$. Spheres represent A-site Ca cations. Dark polyhedra represent B-sites preferentially occupied by Nb^{5+}; light polyhedra, by Ca^{2+}; stippled polyhedra are mixed Ca/Nb sites. Note the similarity between the 1:1 and $\mathbf{LT}_{1/4}$ ordered arrangements.

TABLE 12
Microwave Dielectric Properties of Different $Ca_4Nb_2O_9$ Polymorphs

Phase	Bulk density	f (GHz)	ε^a	$\tan\delta^a$	Qf (GHz)	$\tau_f{}^a$ (ppm/°C)
1:1	0.88	9.15	33	5.8×10^{-4}	16,000	−4
$\mathbf{LT}_{1/4}$	0.89	8.84	32	4.5×10^{-4}	20,000	−7
2:1	0.89	10.63	28	4.4×10^{-4}	24,000	−40

Note. Both ε and $\tan\delta$ values are corrected to theoretical density.
[a] The uncertainty in the presented values of bulk density is of about 2%. The uncertainties for the values of permittivity (ε) and dielectric loss ($\tan\delta$) estimated from measurements on three independent specimens are 4 and 3%, respectively, and are dominated by the uncertainty in measured density. The uncertainty in the measured temperature coefficient of the resonant frequency is of about 2 ppm/°C.

For $Ca_3(CaNb_2)O_9$, the presence of large Ca cations on the B-sites is expected to create additional *lattice stresses*, as reflect by a small value of the tolerance factor $t = (R_A + R_O)/\sqrt{2}\,(R_B + R_O) = 0.85$ calculated for a random occupancy of Ca + Nb on the B-sites. Thus, for perovskite-type $Ca_3(CaNb_2)O_9$, the A(Ca)–O bonds are expected to be stretched while the B(Ca)–O bonds are compressed. The tensile lattice A–O bond stresses in perovskite structures are typically lowered by the displacive phase transition(s) which involves rotation of $[BO_6]$ octahedra; octahedral tilting is accompanied by distortion of the oxygen coordination sphere around the A-cation with displacements of the A-cations from their ideal positions. The tilting transition(s) temperature in $Ca_3(CaNb_2)O_9$ previously was determined to be between 1500 and 1600°C (7), which is higher than the temperatures of either $1{:}1 \rightarrow \mathbf{LT}_{1/4}$ or $1{:}1 \rightarrow 2{:}1$ transitions. According to the present results, the distribution of A(Ca)–O bond distances remains almost unaffected by the subsequent changes in the B-cation ordering: small differences in BVS calculated for the A-sites in both structures can be considered as insignificant.

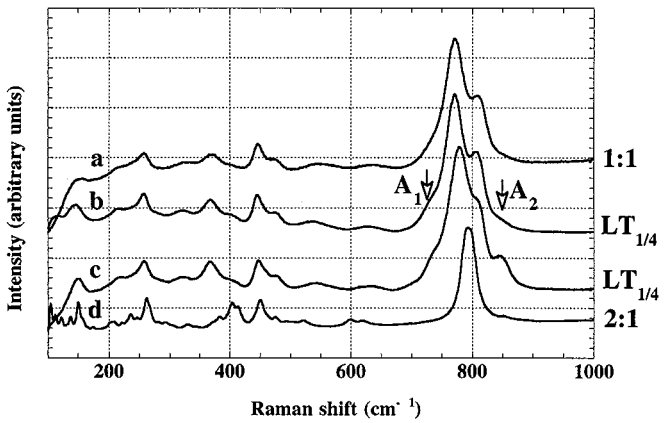

FIG. 8. Raman spectra of the powder specimens containing (a) 1:1 $Ca_4Nb_2O_9$ polymorph, (b) $\mathbf{LT}_{1/4}$ $Ca_4Nb_2O_9$ polymorph, (c) $\mathbf{LT}_{1/4}$ polymorph at composition $0.79CaO{:}0.21Nb_2O_5$, and (d) 2:1 ordered $Ca_4Nb_2O_9$ polymorph. The spectrum of the $\mathbf{LT}_{1/4}$ phase is different from that of the 1:1 polymorph by the presence of peaks A_1 and A_2. Nevertheless, the Raman spectra of both the 1:1 and $\mathbf{LT}_{1/4}$ polymorphs are more similar to each other as compared to that of the 2:1 polymorph.

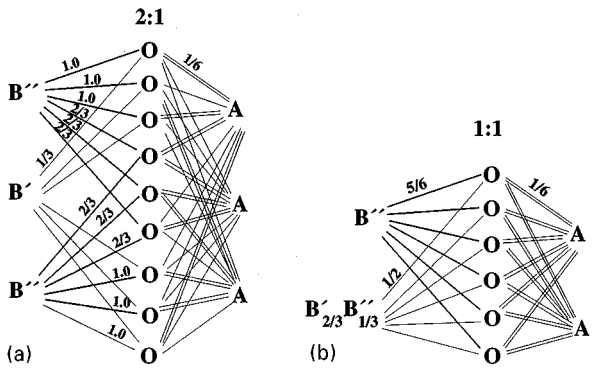

FIG. 9. Bond graphs for the 2:1 (a) and 1:1 (b) ordered B-cation arrays with the $AB'_{1/3}B''_{2/3}O_3$ stoichiometry, where $A = Me^{2+}$, $B' = Me^{2+}$, and $B'' = Me^{5+}$. The bond valences predicted from the bond valence sum requirements about O^{2-} are indicated. The ideal bond valences for the A (coordination number CN = 12), B′ (CN = 6), and B″ (CN = 6) cations are $\frac{1}{6}$, $\frac{1}{3}$, and $\frac{5}{6}$, respectively. Thus, the bond graph of the 2:1 ordered structure predicts off-center displacements of B″-cations toward B′-cations to compensate relatively weak B′–O bonds. No such displacements are expected in the 1:1 ordered array.

The effect of changing the type of cation ordering on the B-cation environments is demonstrated in Fig. 10, which shows the distributions of B–O bond distances for the 2:1 (Fig. 10a), $\mathbf{LT}_{1/4}$ (Fig. 10b), and 1:1 (Fig. 10c) $Ca_4Nb_2O_9$ polymorphs. Rietveld refinement provided an explicit distribution of the B–O bond distances only for the 2:1 ordered structure where either Ca or Nb occupy each of the nonequivalent B-sites. The distribution (Fig. 10a) features three segments, encompassing $\frac{1}{3}$ of the total number of bonds each, and centered about 1.90, 2.10, and 2.27 Å, respectively. Two shorter lengths correspond to the highly distorted $[NbO_6]$ octahedra, while the longest one occurs in the nearly regular $[CaO_6]$ octahedra. The Ca–O bonds are significantly shorter than those predicted from the sum of ionic radii (2.4 Å); a strong residual compressive strain for these bonds is reflected in the abnormally large deviation of the BVS (2.6 v.u., as seen in Table 9) from the ideal value of 2 v.u. In the 1:1 ordered structure, the experimentally determined bond distances for the two nonequivalent $B' = Ca_{2/3}/Nb_{1/3}$ and $B'' = Nb$ positions refer to the average structure only. Nevertheless, this distribution can be reconstructed by making a few assumptions as follows. The $[CaO_6]$ and $[NbO_6]$ octahedra associated with the mixed B′-sites are connected exclusively to the $[NbO_6]$ (B″-site) octahedra (Figs. 4a and 7). Therefore, both Ca–O and Nb–O bond distances associated with the B′-site must have

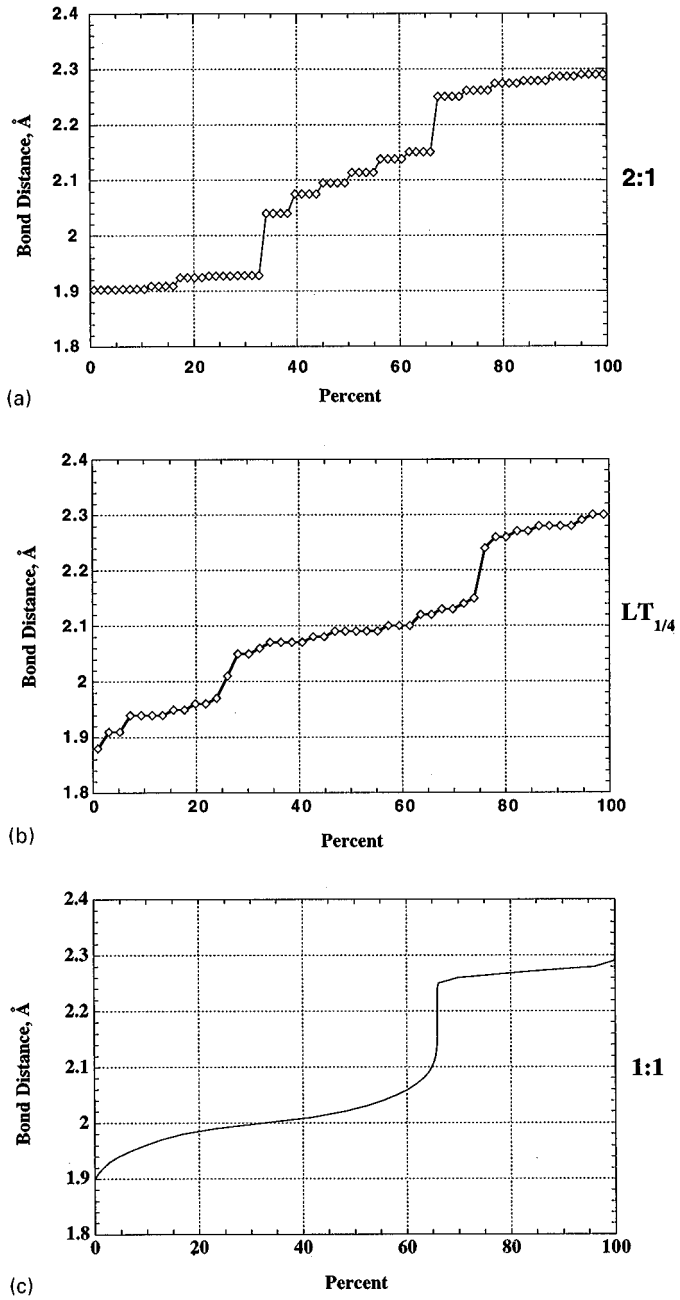

FIG. 10. B–O bond distance distributions for the 2:1 (a), $\mathbf{LT}_{1/4}$ (b) and 1:1 (c) structures. The distribution for the 1:1 ordered structure was reconstructed using the refined average bond distances and a few assumptions, as described in the text. The plots for both 2:1 ordered and $\mathbf{LT}_{1/4}$ structures represent the refined experimental bond distances.

narrow distributions with the statistical average of their mean values equal to $\bar{R}_{\mathrm{Ca/Nb-O}} = (0.67R_{\mathrm{Ca-O}} + 0.33R_{\mathrm{Nb-O}})$. This value was observed to be 2.19 Å experimental (Table 5). The mean B′-site Ca–O bond distance in the 1:1 structure is expected to be similar to that observed in the 2:1 ordered polymorph (2.27–2.28 Å) since the local environments of the $[CaO_6]$ octahedra are similar in both structures. Then, the mean Nb–O distance (B′-site) can be estimated as [(2.19 Å)–(0.67)(2.28 Å)]/0.33 = 2.00 Å. In contrast, the Nb–O distances in the B″-site $[NbO_6]$ octahedra, which are connected anisotropically to both $[CaO_6]$ and $[NbO_6]$ units, must have a broader distribution. We assumed that the Nb–O distances for the B″-site are statistically distributed between the minimum (1.9 Å) and the maximum (2.15 Å) values observed for the $[NbO_6]$ octahedra in the 2:1 structure. The resulting distribution of the B–O distances in the 1:1 ordered structure is illustrated schematically in Fig. 10c. For the $\mathbf{LT}_{1/4}$ structure, the bond distances determined experimentally (Fig. 10b) represent more closely the actual distribution: a very small degree of disorder on six of the eight B-sites can be neglected, while taking into account a disorder on the remaining two B-sites will only slightly modify the distribution. As seen in Fig. 10, the distribution of bond distances in the $\mathbf{LT}_{1/4}$ structure is intermediate between those in the 1:1 and 2:1 structures, respectively.

Comparison of the three B-site to oxygen bond distance distributions in Fig. 10 indicates that the changes in the cation arrangements $1{:}1 \rightarrow \mathbf{LT}_{1/4} \rightarrow 2{:}1$ mainly affect the distribution of Nb–O bond distances with a progressively increasing average distortion of the Nb environment. As a result, the fraction of highly compressed Nb bonds in the 2:1 ordered structure is significantly larger than in either the 1:1 ordered or $\mathbf{LT}_{1/4}$ polymorphs. The $\mathbf{LT}_{1/4}$ cation array apparently provides a compromise between the trend to complete segregation of the Ca and Nb cations on different $\{1\,1\,1\}_c$ B-cation planes, and increasing average distortion of the Nb environment associated with such cation rearrangements. According to the present observations, the increasing average distortion around the higher valent B″-cation, accompanied by the increased *fraction* of strongly *compressed* B″–O bonds, correlates with the decrease in dielectric constant and change of τ_f toward more negative values (positive for τ_ε).

The results obtained here are consistent with the observations made by Takahashi *et al.* (22), who studied the effects of changes in the type of B-cation ordering on low-frequency dielectric properties in the $(Sr_{1-x}Ba_x)(Sr_{1/3+y}Ta_{2/3-y})O_{3-\delta}$ system. In their study, the 1:1 and the

TABLE 13
Fraction of Types of B–O–B Links in the $AB'_{1/3}B''_{2/3}O_3$ Structure with Different Arrangements of B-cations

	Fraction of B–O–B links		
Cation arrangement	B′–O–B′	B″–O–B″	B″–O–B′
Disordered	0.1111	0.4444	0.4444
1:1 Ordered	0	0.3333	0.6667
2:1 Ordered	0	0.3333	0.6667

2:1 arrangements of cations on the B-sites were obtained by varying the Sr/Ba ratio on the A-site, and the 2:1 ordered structures consistently exhibited lower dielectric constant and more positive τ_ε as compared to those with 1:1 ordering. A decrease in dielectric constant and the change of τ_ε toward more positive values have also been reported to accompany an order → disorder transition in a number of complex perovskites (23, 24). A transition from disordered to either of the ordered structures (1:1 or 2:1) modifies the fractions of chemically distinct B–O–B links as given in Table 13. In particular, the B′–O–B′ links ($B' = Me^{2+}$) with relatively weak B′–O bonds disappear upon a disorder → order transition, with a simultaneous increase in the fraction of the B″–O–B′ links containing strengthened B″–O bonds, which is similar to the effect identified in the present study. Tilting phase transitions in perovskites have similar effects on τ_ε, changing it to a more positive value (25); octahedral tilting distorts the A-cation environment with consequential shortening of some A–O bonds. The similarities discussed suggest a general correlation between distortion of the environment of a stretched cation (either A or B), accompanied by the increased fraction of compressed cation–oxygen bonds, and change of τ_ε; however, more data need to be accumulated before a final conclusion is made.

CONCLUSIONS

Dielectric permittivity (ε) and temperature coefficient of resonant frequency (τ_f) were found to systematically depend on the type of B-cation ordering in studies of three perovskite-like $Ca_4Nb_2O_9$ polymorphs. The completely ordered 2:1 structure exhibited lower ε and more negative τ_f as compared to both the 1:1 and $\mathbf{LT}_{1/4}$ polymorphs, which feature partial ordering of the B-cations; the changes in τ_f were especially significant. Detailed structural analyses confirmed that in all three $Ca_4Nb_2O_9$ polymorphs the B-cation ordering is combined with $b^-b^-c^+$ octahedral tilting with very similar magnitudes of the tilting angles. The structural model for the $\mathbf{LT}_{1/4}$ structure, which represents a new type of B-cation ordering, was derived from the qualitative analysis of transmission electron microscopy and X-ray powder diffraction data, and subsequently validated by Rietveld refinement. According to this model, the $\mathbf{LT}_{1/4}$ structure is derived from the 1:1 ordered structure by partial ordering of Ca and Nb cations on those B-sites which were occupied by a random $Ca_{2/3}Nb_{1/3}$ mixture in the 1:1 ordered array. Detailed analysis of the structural results indicated that an increasing average out-of-center *distortion* around the B″ = Nb cation sites is the *major* crystal-chemical effect accompanying the change in ordering from the 1:1 to the 2:1 type; the distortion was shown to be driven by bond valence sum requirements. The $\mathbf{LT}_{1/4}$ arrangement exhibits average distortion intermediate between that observed in the 1:1 and 2:1 ordered structures, which is consistent with its dielectric properties and Raman spectra. For a given chemical composition the increasing fraction of strongly compressed (strengthened) B″–O bonds, where B″ denotes the higher-valent Nb cations, correlates with a decrease in dielectric constant and change of τ_f toward more negative values.

ACKNOWLEDGMENTS

The authors are grateful to J. M. Loezos and D. B. Minor for specimen preparation. The assistance of B. A. Reisner and J. P. Cline with diffraction experiments is greatly appreciated.

REFERENCES

1. S. Kawashima, M. Nishida, I. Ueda, and H. Ouchi, *J. Am. Ceram. Soc.* **66**(6), 421–423 (1983).
2. K. Matsumoto, T. Hiuga, K. Takada, and H. Ichimura, "Proceedings, 6th IEEE International Symposium on Applications of Ferroelectrics, NY," pp. 118–121. 1986.
3. F. Galasso and J. Pyle, *Inorg. Chem.* **2,** 483 (1963).
4. P. K. Davies, J. Tong, and T. Negas, *J. Am. Ceram. Soc.* **80**(7), 1727–1740 (1997).
5. M. A. Akbas and P. K. Davies, *J. Am. Ceram. Soc.* **81**(3), 670–676 (1998).
6. M. Hervieu, F. Studer, and B. Raveau, *J. Solid State Chem.* **22,** 273–289 (1977).
7. I. Levin, L. A. Bendersky, J. P. Cline, R. S. Roth, and T. A. Vanderah, *J. Solid State Chem.* **150,** 43–61 (2000).
8. A. M. Glaezer, *Acta Crystallogr. B* **31,** 2129–2130 (1975).
9. R. S. Roth, unpublished results (1999).
10. A. C. Larson and R. B. Von Dreele, "General Structure Analysis System," Report LAUR 86-748. Los Alamos National Laboratory, NM, 1994.
11. R. G. Geyer, J. Baker-Jarvis, T. A. Vanderah, and J. Mantese, *Adv. Dielectr. Ceram. Mater.* 115–129.
12. H. F. Kay and P. C. Bailey, *Acta Crystallogr.* **10,** 219 (1957).
13. W. A. Groen, F. P. F. van Berkel, and D. J. W. Ijdo, *Acta Crystallogr. C* **42,** 1472–1475 (1986).
14. R. D. Shannon, *Acta Crystallogr. A* **32,** 751–767 (1976).
15. I. D. Brown and D. Altermatt, *Acta Crystallogr. B* **41,** 244–247 (1985).
16. I. G. Siny, R. S. Katiyar, and A. S. Bhalla, *J. Raman Spectrosc.* **29,** 385–390 (1998).
17. I. G. Siny, R. Tao, R. S. Katiyar, R. Guo, and A. S. Bhalla, *J. Phys. Chem. Solids* **59**(2), 181–195 (1998).
18. H. Tamura, D. A. Sagala, and K. Wakino, *Jpn. J. Appl. Phys.* **25**(6), 787–791 (1986).
19. M. Kunz and I. D. Brown, *J. Solid State Chem.* **115,** 395–406 (1995).
20. I. D. Brown, *Acta Crystallogr. B* **48,** 553–572 (1992).
21. H. Vincent, Ch. Perrier, Ph. I'Heritier, and M. Labeyrie, *Mater. Res. Bull.* **28,** 951–958 (1993).
22. J. Takahashi, T. Fujii, S. Shimada, and K. Kodaira, *J. Eur. Ceram. Soc.* **19,** 1089–1093 (1999).
23. I. T. Kim, Y. H. Kim, and S. J. Chung, *Jpn. J. Appl. Phys.* 1 **34**(8A), 4096–4103 (1995).
24. R. J. Cava, J. J. Krajewski, and R. S. Roth, *Mater. Res. Bull.* **34**(3), 355–362 (1999).
25. E. L. Colla, I. M. Reaney, and N. Setter, *J. Appl. Phys.* **74**(5), 3414–3425 (1993).